Title

THE DEVELOPMENT OF A THREE-DIMENSIONAL VALENCE RAND STRUCTURE IN Ag OVERLAYERS ON Cu(001)

Author

Tobin, J.G.

Publication Date

1986-09-01

Lawrence Berkeley Laboratory
UNIVERSITY OF CALIFORNIA

Materials & Molecular Research Division

Submitted to Physical Review B

THE DEVELOPMENT OF A THREE-DIMENSIONAL VALENCE BAND STRUCTURE IN Ag OVERLAYERS ON Cu(001)

J.G. Tobin, S.W. Robey, L.E. Klebanoff, and D.A. Shirley

August 1986

Prepared for the U.S. Department of Energy under Contract DE-AC03-76SF00098

DISCLAIMER

LBL-15134

THE DEVELOPMENT OF A THREE-DIMENSIONAL VALENCE BAND STRUCTURE IN Ag OVERLAYERS ON Cu(001)

J.G. Tobin,* S.W. Robey,† L.E. Klebanoff,‡ and D.A. Shirley

Materials and Molecular Research Division
Lawrence Berkeley Laboratory
and
Departments of Chemistry and Physics
University of California
Berkeley, California 94720

*Present Address: Department of Chemistry, University of Wisconsin, Madison, Wisconsin 53706.
†Present Address: IBM, T. J. Watson Research Center, Yorktown Heights, NY 10598
‡Present Address: National Bureau of Standards, B206/220, Gaithersburg, Maryland 20899.

THE DEVELOPMENT OF A THREE-DIMENSIONAL VALENCE BAND STRUCTURE IN Ag OVERLAYERS ON Cu(001)

J.G. Tobin,* S.W. Robey, L.E. Klebanoff, and D.A. Shirley

Materials and Molecular Research Division
Lawrence Berkeley Laboratory
and
Departments of Chemistry and Physics
University of California
Berkeley, California 94720

ABSTRACT

Using monochromatic synchrotron radiation over the energy range of 6-32 eV, the development of the valence band electronic structure of Ag overlayers on Cu(001) was followed with angle-resolved photoelectron spectroscopy. The electronic structure was observed to be two-dimensional for a single adlayer of c(10x2) Ag/Cu(001). By five layers of coverage, the silver valence band structure was bulk-like, three-dimensional and very similar to that of Ag(111).

I. INTRODUCTION

Over the last several years, a number of photoemission experiments and calculations have investigated the properties of metal overlayer-metal substrate systems.[1] In particular, experimental[2] and theoretical[3] efforts have been made to elucidate the effect of thickness upon the electronic structure of thin metal slabs. An earlier Communication[4] gave a brief report of the development from 2-dimensional to 3-dimensional valence electronic structure in the silver overlayer of the all-metal system c(10x2) Ag/Cu(001). A full report of the 2-dimensional silver valence band structure at monolayer coverages was presented in Ref. 1. In this paper, we present a more complete discussion of the angle-resolved photoemission experiment at higher exposures. This synchrotron-radiation based study documents the development of the electronic structure in the overlayer from 2-dimensional to 3-dimensional bulk behavior.

The system c(10x2) Ag/Cu(001) was chosen for several reasons, including its layer-by-layer growth pattern at low coverages and the expectation that this would continue at higher exposures, the ease of preparation, the stability of its constituents in vacuo, the limited overlap in energy of the valence bands of adsorbate and substrate, and the fact that Ag(111) has been studied in detail.[1,5] This system also has the distinct advantage of commensurate but non-epitaxial growth: Low Energy Electron Diffraction (LEED) as well as Auger Electron Spectroscopy (AES) can therefore be used to follow the growth pattern. The overlayer of the c(10x2) Ag/Cu(001) system has a slightly-

strained hexagonal geometrical structure. It seemed reasonable to expect that at higher coverages it would approach the geometrical and electronic structure of the (111) face of crystalline silver. This behavior was in fact observed at the rather low coverage of 5 ML.

The remainder of this paper is organized as follows: Section II is a description of the experimental details, Section III contains photoemission results and Section IV is a discussion of those results. Section V contains a summary of conclusions.

II. EXPERIMENTAL

The first part of this section is devoted to the details of the photoemission experiments. The second part deals with the LEED/AES calibration performed to allow accurate and reproducible preparation of evaporated samples.

A. The Photoemission Experiments

The measurements were made at the Stanford Synchrotron Radiation Laboratory (SSRL) on Beam Line I-2, over the energy range of $h\nu$ = 6-32 eV, with an angle-resolved photoelectron spectrometer described previously.[6] The base pressure during the experiment was 1×10^{-9} Torr and operation of the Ag evaporator had essentially no effect upon the chamber pressure. Fortunately, Ag and Cu metal surfaces are both relatively nonreactive and thus less susceptible to contamination. Spectra taken at SSRL under these conditions were consistent with those collected in-house using HeI and NeI lamp sources, in a superior vacuum environment (base pres = 2×10^{-10} Torr).[1]

The Cu(001) crystal was cut and polished to within ±1° of the (001) face and chemically polished before introduction into the vacuum system. The crystal was aligned in-situ using LEED and laser autocollimation to a precision of better than ±1°. The crystal had a specular finish and sharp 1x1 LEED spots, indicative of surface ordering. Evaporations were performed using a thermal source of Ag atoms which was monitored with a quartz crystal microbalance. The source and microbalance were contained inside a shielded assembly with a shutter to allow time-controlled evaporations.

Room temperature Ar ion etching at pressures of 10^{-5} Torr was used to remove evaporated Ag, monitored by Auger spectroscopy, but cycles of heating to between 500°C and 600°C and cooling with continuous sputtering were used to remove residual contaminants. A final annealing to above 500°C was used to order the clean Cu(001) crystal, at which point contaminant levels were such that neither oxygen nor sulfur was detectable and the C/Cu Auger intensity ratio was 0.004--all measured using a four grid LEED system in a retarding-field mode.

Possible sulfur impurities were detected at lower exposures but after extended photoemission measurements and all evaporations, the sulfur and oxygen impurities were barely detectable. Any possible carbon Auger line was obscured by an Auger line of Ag at 260 eV.

The analyzer resolution was kept at 60 meV (10 eV pass energy) throughout the experiment, but the monochromator contribution varied with photon energy and slit width.[7] It is assumed that the full-width-at-half-maximum (FWHM) linewidths add in-quadrature. For $6\ \text{eV} \leq h\nu \leq 24\ \text{eV}$, $65\ \text{meV} \leq \Delta E\ (\text{FWHM}) < 100\ \text{meV}$. For $h\nu = 26$ eV, $\Delta E = 111$ meV; $h\nu = 28$ eV, $\Delta E = 169$ meV; $h\nu = 30$ eV, $\Delta E = 191$ meV; $h\nu = 32$ eV, $\Delta E = 215$ meV. The half-angular acceptance of the electrostatic analyzer was always $\pm 3^\circ$ or less.

All the photoemission spectra were taken with p-polarized radiation, usually at normal emission. The polarization was in the horizontal plane, as were the Poynting vector of the light, the surface normal and the (110) plane of Cu(001). The angle of incidence of the light was 60° with respect to the normal. The single domain[1] of the

c(10x2) Ag was oriented such that the polarization and the $\overline{\Gamma} - \overline{\Sigma} - \overline{M}$ direction of the hexagonal Surface Brillouin Zone were in the same plane, as shown in Figure 1.

The binding energies (B^F) were measured with respect to the Fermi energy (E_F), which was determined separately in each individual spectrum as the point of maximum slope in the rise from background to the initial s-p plateau or band feature. The spectrometer work function was determined as a function of exposure. The values found, including the RMS scatter as the error, are shown in Table I. The actual value of the spectrometer work function is, of course, relatively unimportant. The figures of merit are the small RMS scatter at each coverage and the relatively small variation as the coverage was increased. The Ag(111) measurements were made on a later separate experimental run.[5] They are included in Table I for comparison.

B. LEED/Auger Calibration

AES and LEED were used to calibrate the quartz microbalance thickness monitor, as previously discussed in Ref. 1. In a layer-by-layer growth pattern, a discontinuity in the slope of the ratio of adsorbate to substrate intensities is to be expected at one monolayer coverage. Ratios were used because of inaccuracies introduced into absolute measurements by movement of the crystal during the experiment. At a slightly higher coverage than that corresponding to the discontinuity in the slope of the Ag(350 eV)/Cu(60 eV) ratio, the first c(10x2) LEED spots were observed. The quartz microbalance was thus calibrated for

sub- and multi-atomic layer coverages of Ag on the Cu(001) crystal and used as a guide during evaporations.

As a check on the accuracy of the quartz microbalance, derivative intensity measurements were made of each sample for the Auger lines of Cu MVV (60 eV), Ag MNN (350 eV) and Cu LMM (920 eV) and compared to the original measurements, Ag(350)/Cu(60) and Ag(350)/Cu(920), taken during calibration. The Cu (920 eV) measurements were necessary because at higher exposures the Cu (60 eV) is drastically attenuated due to its much shorter mean free path. The results proved to be generally internally consistent. The estimate of the accuracy is typically ±20% of the exposure.

LEED observations made at higher coverages (2-5 ML) showed that the pattern was remaining essentially the same as that at 1 ML, but that the adsorbate spots were increasing in number, intensity and sharpness relative to substrate spots, with a possible removal of the splitting of some of the adsorbate spots. In an earlier LEED/AES experiment,[1,7] it had been observed that at coverages around 10 ML the copper substrate spots were no longer visible and the adsorbate spots were qualitatively the same as those of a Ag(111) 1x1 pattern. The normal-emission HeI photoemission spectrum collected at this exposure was very similar to that of the Ag(111) spectrum of Spears et al.[8]

Finally, the ratio of the photoemission intensities of the silver and copper valence features was used to check the results of the LEED/AES experiments. In general, they confirmed the LEED/AES results. The

relative intensities of the silver and copper valence bands were normalized to that for 1 ML. An empirical function which consisted of a scaled and shifted clean copper spectrum was used to fit the residual copper features. The silver intensity was obtained by subtracting the empirical function from the spectrum and then summing the intensity of the individual channels. These results were then compared to the predictions of a simple model including attenuation effects, a description of which is in Appendix 1. A summary is given in Table II. Taken all together, the ratios are reasonably consistent. However, these results must be approached with caution: the cross sections of the silver valence bands may be changing with exposure, as well as the illumination and magnitude and direction of the polarization of each layer.

As discussed in Ref. 1, this Cu(001) sample exhibited only one of the two possible orthogonal domains of the c(10x2) structure. This may have been caused by the slight misalignment of ($\pm 1^{\circ}$) the crystal face from (001) and the subsequent breakdown of the degeneracy of the [100] and [010] directions due to steps. Because of the localized sampling of the photoemission process, the presence or absence of the second domain is not crucial.

III. PHOTOEMISSION RESULTS

Photoemission spectra were collected for photon energies in the range 6-32 eV from samples with Ag coverages between 1/2 and 5 monolayers and for clean Cu(001) and Ag(111).[5] A complete presentation of these spectra is available in Ref. 7. All copper and Ag/Cu(001) spectra in figures 2-6 were collected at normal emission with the experimental geometry illustrated in Figure 1, as were the Ag(111)[5] spectra in Figs. 2-6. This was to facilitate the comparison of the c(10x2) spectra with those of the Ag(111). It is especially important that the surface Brillouin zones of the Ag(111) and the c(10x2) Ag were oriented the same with respect to the Poynting vector and polarization of the radiation. While all of the data were used in the analysis, only a few particularly representative spectra will be reproduced here.

Figure 2 shows spectra taken at $h\nu$ = 6, 7 and 8 eV. A major point of interest here is the development of a precursor to the Ag(111) surface state that occurs near E_F. This is most easily seen in the 7 and 8 eV spectra, where the silver state grows in continuously, while the copper features are slowly diminishing. Also of interest is the absence of a silver overlayer feature corresponding to Band 6 in Ag(111), which is present at $h\nu$ = 6, 7 and 8 eV at B^F near 1-2 eV. This will be discussed in detail in the next section.

As the photon energy is increased through our experimental range, the element of volume in $\vec{k}$-space which the photoemission process samples moves toward the centers of the three-dimensional Brillouin zones

of both silver and copper. As would be expected from the known band structures of bulk Cu and Ag, the overlap of adsorbate and substrate features thereupon is observed to decrease. This is apparent in Figure 3, where spectra taken with $h\nu = 14$ eV are shown. At $h\nu = 14$ eV, a trio of silver features near $B^F = 4.6$ eV, a shoulder, a peak and another shoulder, are easily visible as is a weaker feature at higher coverage and binding energy, near $B^F = 5.5$ eV. The high binding energy shoulder at 4.9 eV may be a copper feature in the $h\nu = 14$ eV spectra. At binding energies above that, peaks are not identifiable, except at the highest exposures.

For $h\nu \geq 14$ eV, the higher exposure c(10x2) Ag/Cu(001) surfaces have spectra that are very similar in appearance to the bulk Ag(111) spectra, if the copper features at lower binding energies are ignored. This is emphasized by the decreasing electron escape depth with increasing electron (and thus photon) energy, which serves to amplify the Ag overlayer/Cu substrate spectral intensity ratio. The absence of Band 6 and hence the failure of the lower photon energy spectra of the higher exposure samples to closely mimic the Ag(111) spectra will be discussed in the next section.

In Figure 4, the spectra taken at $h\nu = 24$ eV are shown. The features at $B^F = 4.3$, 4.7, 4.8, 5.6, 6.1, and 6.9 eV are present at photon energies of 21-24 eV, with the shoulder-peak near 4.7 eV being among those most prominent. The feature at $B^F = 6.9$ eV at 5 ML is absent at $h\nu = 23$ and 24 eV, lost in the broadening tail of the other peaks. In these spectra the peak at 4.3 eV is quite strong,

particularly at coverages of 2 and 3 monolayers of silver. It is enveloped by the broadening 4.8 eV peak at higher exposures, where it becomes a shoulder on the leading edge of the silver d-bands. Also, the peaks at greater binding energies are undergoing a relative increase in intensity, particularly at exposures of 4 and 5 monolayers, thus mimicking the behavior of the peaks in the Ag(111) spectra. This contributes to the difficulty in observing the feature at B^F = 6.9 eV at 5 ML.

The spectra taken at $h\nu$ = 26, 28, 30, and 32 eV continue the trends observed at $h\nu$ = 21-24 eV, but the degraded resolution causes a larger sampling of k-space and more averaging over the Brillouin zone. This is illustrated by the $h\nu$ = 28 eV spectra in Figure 5. The most striking features are those at a coverage of two monolayers. As above, a strong separate peak at B^F = 4.2 eV is present, before it becomes a shoulder at higher exposures. Again there is a very strong resemblance between the silver overlayer features at higher exposures and the Ag(111) spectrum.

At photon energies of 26 eV and above, a broad feature is present in the Ag(111) spectra at a kinetic energy of 17 eV with respect to the Fermi level ($B^F = h\nu - 17$ eV). The highest exposure c(10x2) Ag/Cu(001) samples also displayed this very broad, weak peak at $h\nu \geq 28$ eV, as indicated by the arrows in Figure 6.

IV. DISCUSSION

We discuss dispersive behavior in the Ag overlayer in part A, followed by a comparison with Ag(111) in part B.

A. Dispersive Behavior

The above data were collected over the range of $h\nu$ = 6-32 eV with the electron emission along the surface normal. The component of photoelectron momentum parallel to the surface is zero and the component perpendicular to the surface is equivalent to the total crystal momentum. Thus this is a direct probe of the dependence of the dispersion relations upon the perpendicular component of the crystal momentum and a test for three dimensionality in the valence-band dispersion. Energy conservation can be expressed in the following form:

$$B^F = h\nu - KE - \varphi = h\nu - KE_{AN} - \varphi_{AN}, \qquad (1)$$

with $KE(KE_{AN})$ the kinetic energy in the vacuum (analyzer), $h\nu$ the photon energy, B^F the binding energy with respect to the Fermi level, and $\varphi(\varphi_{AN})$ the work function of the crystal (spectrometer/analyzer).

For normal emission from Ag(111), the final state is a particularly well-defined, single state.[5] The final state of the photoelectrons emitted from the c(10x2) Ag adlayers is not well understood. To avoid any unnecessary and possibly prejudicial assumptions concerning the final state, the comparison of the overlayer and Ag(111) dispersion relations will be made empirically by plotting the binding energies versus photon energy. Figures 7-11 are plots of the B^F values of the silver features versus photon energy for 1, 2, 3, 4 and 5 ML

coverages, respectively. Figure 12 is a plot of the Ag(111) data versus photon energy. With respect to Figures 7-11, separating the silver adsorbate from the copper substrate features was sometimes difficult. Any silver feature overlapping with the strong copper d-band peaks near B^F = 2-3 eV was essentially lost. On the other extreme, the weak copper feature at $B^F \geq 5$ eV caused significant problems in assignment of weak peaks and shoulders in the region. Nevertheless, the high energy and angular resolutions used made peak assignment possible.

A careful examination of the binding energies (B^F) with respect to the Fermi level shows marked changes in going from one to two to three monolayers and demonstrates a convergence toward Ag(111)-like behavior at coverages of 4 and 5 ML. Each of the lower coverages will be discussed separately.

One Monolayer. At one monolayer coverage, the geometrical structure of the adlayer is known to be an atomic monolayer film and the d-band electronic structure of the adlayer has been shown to be primarily two dimensional.[1] In Figure 7, the silver features of the one monolayer coverage sample are shown not to disperse with photon energy and are thus independent of $k_\perp$, the perpendicular component of momentum. The scatter in the points simply reflects the difficulty in determining the B^F values of these weak features [particularly in light of the decreased scatter of the flat bands of Figure 8]. This is direct confirmation of the 2-dimensional electronic structure found in the off-normal bandmapping experiment.[1] As discussed in

that paper, if the contribution of the Cu(001) surface is neglected, then the dominant symmetry of the potential will be C_{6v} at one monolayer. Also as described in Ref. 1, a single group analysis is appropriate. The features observed are attributed to the $A_1(C_{6v})d_{3z^2-r^2}$ state (B^F = 4.2 eV), the spin-orbit-split $E_1(C_{6v})d_{xz,yz}$(B^F = 4.8 eV) and the $A_1(C_{6v})_s$ state (B^F = 6.3 eV). Weak features near B^F = 3,5, 5.2 and 8 eV are observed in some of the spectra. These are due to transitions of the underlying Cu(001) substrate. The symmetry forbidden transition originating from the silver $E_2(C_{6v})d_{xy,\ x^2-y^2}$ state is not observed.[1]

Two Monolayers. At two monolayers (Figure 8), C_{3v} symmetry would be present. Experimentally, the bands are still observed to be flat and qualitatively the same as for one monolayer, except that the lowest band (greatest B^F) has shifted from B^F = 6.4 eV at one monolayer to 6.7 eV at 2 monolayers. This may be a manifestation of Density-of-States (DOS) broadening in going from two- to three-dimensionality, since band width should increase with slab thickness.[3]

Under C_{3v} symmetry, the representations and selection rules are only slightly different, with the above mentioned states essentially the same. Operating under C_{6v} selection rules, the transition from the E_2 state is forbidden. In going from 1 to 2 ML, this E_2 (C_{6v}) state becomes $E(C_{3v})$, which is symmetry allowed. A weak feature near B^F = 5.4 eV is seen at some photon energies at coverages of 1 and 2 ML, but it is believed to be due to the tail of the Cu(001) feature at

B^F = 5.2 eV. From the off-normal study,[1] it is known that the E_2 state should be in this region of B^F. Perhaps it is obscured by the copper peak or the C_{6v} contribution to the C_{3v} potential dominates it to the extent that the transition is still essentially forbidden. ($\vec{A}.\vec{p}$ vectoral alignment also militates against a large partial cross section at normal emission, since it is only allowed for the in-surface-plane component of the polarization, $\vec{A}_{\parallel}$. However the same is true for the E_1 ($d_{xz,\ yz}$) state, which nonetheless has significant intensity.)

The features near B^F = 4.7 and 4.9 eV at 1 and 2 ML are assigned as the spin-orbit-split-doublet of the $Y_2^{\pm 1}$ [$E_1(C_{6v})$ or $E(C_{3v})$] state. The observed splitting and RMS scatter at 1 ML is 0.26 ± 0.05 eV, and at 2 monolayers it is 0.25 ± 0.04 eV. These values agree well with that of 0.24 eV found in the resonance lamp experiment for coverages near one monolayer.[1]

Three Monolayers. At three monolayers (Figure 9), qualitatively new behavior is observed. For all adlayers thicker than two monolayers, there will always be a C_{3v} symmetry interface layer and a C_{3v} symmetry surface layer sandwiching octahedral symmetry layers between them. This is assuming a layer-by-layer and face-centered-cubic growth pattern. At three monolayers, the first octahedral layer will be present and experimentally two new bands are observed. We associate these with transitions allowed under double group, perturbed octahedral selection rules.[1] One, near B^F = 5.5 eV, overlaps with the copper substrate feature but is much stronger than before. The other,

at B^F = 6.1 eV, has no substrate complications. Moreover, the band structure at 3 ML is distinctly bulk-like in that there are now six separate levels between B^F = 4.0 eV and B^F = 7.0 eV, corresponding to Bands 1-6 of Ag(111) (Figure 12). There may also be the beginning of dispersion in Bands d and e at $h\nu \leq 20$ eV.

The feature at B^F = 4.2 eV is not merely a precursor of one of the bulk bands but appears to develop into a residual $A_1(C_{3v})$ state of the surface layer, and possibly of the interface layer as well. This explains the shoulder (open circles in Figures 11 and 12) seen near 4 eV in the bulk Ag(111) spectra, previously interpreted as being due to indirect transitions.[9] At $h\nu$ = 22-32 eV, this feature can be seen to persist as a separate peak even up to four monolayers, where it finally becomes enveloped in the broadening Bands d and e.

A peak at B^F = 3.5 eV is seen at $h\nu$ = 10-16 eV at coverages of 3-5 ML. It appears to be due to the copper substrate spectral structure, but it may also be a precursor to the dispersive s-p band away from the bulk zone center.

The success of the group theoretical analysis in explaining the new bands at three monolayers is the strongest evidence to date that the growth mode is layer-by-layer beyond 1 ML, at least up to coverages of three monolayers. Considering that only 100-200 atoms are necessary to observe bulk-like effects in Au and Ag clusters,[10,11] the absence of any other bands at one and two monolayer coverages is convincing evidence of their planar nature, and supports the hypothesis of continued layer-by-layer growth.

Four and Five Monolayers. Continuing to the four and five monolayer coverages (Figures 10 and 11), the bands generally remain stationary at $h\nu \geq 26$ eV. However, dispersion is observed in Bands d and e as the photon energy decreases to 10 eV. This mimics what is observed for Ag(111) in Figure 12 and corresponds to the dispersion occurring away from Γ ($h\nu \sim 24$ eV) and toward L ($h\nu < 6$ eV) in the bulk three-dimensional Brillouin zone. The appearance of states near $B^F = 3.5$ eV may be related to the dispersion of the bulk Band 6 up to the Fermi energy near the L point. But regardless of that assignment, the features near $B^F = 4.7$ eV are dispersing steadily in going from $h\nu = 20$ to 10 eV in the four-five monolayer systems. Note that in the 5 ML case, the assignments in Bands d,e, and f have been changed to be consistent with Bands 4,5, and 6 of Ag(111). This is justified in part by the similarity of the 5 ML and Ag(111) spectra.

The gradual, continuous development toward bulk band structure is consistent with a layer-by-layer growth pattern. At the five monolayer exposure, there are approximately 6×10^{15} atoms of Ag per square centimeter and a 5 ML slab would be approximately 13 Å thick. At 5×10^{15} atoms/cm^2, the electronic density of states of the Au clusters studied by Lee et al.[10] is very bulk-like. Assuming hemispherical cluster growth, this implies that bulk behavior is associated with thicknesses or heights of 10-20 Å. In this experiment the perpendicular direction alone is being probed. If significant island formation were occurring in the silver overlayer, thicknesses of twice or more relative to that calculated for the quoted silver exposure could well be expected and

the transition from two- to three-dimensionality would be much more rapid. Also, the continued observation of the $A_1(C_{3v})$ state at B^F = 4.3 eV suggests the existence of large sections of an intact hexagonal topmost layer.

Let us now consider the absence from the overlayer spectra of an intense, sharp feature for Band 6 at $B^F < 4$ eV. The only silver overlayer features near the energy of the Ag(111) Band 6 at $h\nu < 14$ eV are the weak, flat structure at $B^F = 3.5$ eV and the broad, intense precursor to the Ag(111) surface state near E_F. At the other extreme, sharp, intense silver overlayer peaks are seen for $h\nu \geq 14$ eV at $B^F \geq 4$ eV.

The most likely cause of the observed behavior is that interactions with the substrate affect Band 6. Band 6 at $B^F < 4$ eV and the Ag(111) surface state are of s-p character, while Bands 1-6 of Ag(111) at $B^F \geq 4$ eV are mainly of d character. It appears that adsorbate d levels can sometimes behave as isolated core states and not participate in interactions with the substrate.[1] On the other hand, delocalized s and p electrons would be the most likely candidates for interaction with the substrate. Hence, substrate-adsorbate bonding interactions, which must be occurring to some extent, based on the observed stability of the overlayer on the Cu(001) surface, would not perturb the adsorbate d levels ($B^F \geq 4$ eV). Rather they would severely affect the sp states; e.g., Band 6 at $B^F < 4$ eV and the surface state. Note that if all sp states were thus affected, it would preclude hybridization between the d Bands and the sp Band.

B. Development of Ag(111) Spectral Characteristics

Besides the development of normal emission dispersion, several other facets of spectral behavior peculiar to Ag(111) develop in the c(10x2) Ag overlayers.

Band 7 Resonance. A sharp variation in the intensities of the d-Band peaks is observed in Ag(111) through the range $h\nu$ = 21-24 eV. It is caused by the matching of the photon energy and the energy separation between the initial state d-Bands and a flat region of Band 7 near Γ, the center of the bulk Brillouin zone. This is also observed at 4 and 5 ML coverages in c(10x2) Ag.

While it is extremely difficult to fit each peak accurately, it is possible to measure the intensities of the top and bottom halves of the Ag VB. Figure 13 shows a comparison of these integrated intensities for Ag(111)[5] and c(10x2) Ag/Cu(001). It is obvious that the cross-section resonance seen in Ag(111) is also occurring in the adlayers, although to a diminished degree. Qualitatively, the resonance is observable in the raw spectra for the above systems from $h\nu$ = 20 eV to $h\nu$ = 26 eV.

This behavior occurs in Ag(111) at Γ, where atomic effects should dominate. Atomic Ag spectra[12] do show a distinct increase in cross-section magnitude over the energy range $h\nu$ = 17-20 eV. The results over the range of $h\nu$ = 20-27 eV are too incomplete to dismiss the possibility of an atomic cross-section resonance occurring there. However, the resonance is not observed at the lower exposures of the

c(10x2) Ag system and the effect is seen to grow stronger with increasing exposure.

Constant Kinetic Energy Feature. Another feature identified with Ag(111) is the constant kinetic energy peak at 17 eV with respect to the Fermi level. This is also due to the flat region of Band 7 of Ag(111), near the center of the bulk Brillouin zone. Electrons scatter into it, producing a peak that appears to move across the spectra at $B^F = h\nu - 17$ eV for $h\nu = 26$–32 eV.[9] At 28 eV and 30 eV photon energies (Figures 5 and 6), this feature is observable at 4 and 5 monolayers, and at $h\nu = 32$ eV at 5 monolayers. This is a strong indication of bulk-like final state behavior in the silver overlayer.

Surface State. At lower photon energies, $h\nu = 6$–12 eV, the Ag(111) surface state is present near the Fermi level. At some of these photon energies, copper features obscure this spectral region but for $h\nu = 7$–9 eV the development of a precursor surface state is easily seen. Table III contains a summary of surface state data taken from the $h\nu = 8$ eV spectra. (The $h\nu = 8$ eV spectra have a flat Cu substrate background.) The binding energies were determined by visual inspection. The widths were found by fitting the Fermi edge step and surface peak with a gaussian step and a lorentzian peak function multiplied by a Fermi occupation function (T = 300 K). The gaussian step and occupation function were set to the value of the Fermi energy determined by visual inspection and the lorentzian mean was set to the peak energy,

also found by visual inspection. The listed widths are the FWHM of the unabridged lorentzians. Instrumental broadening is insignificant compared to these widths. (The Ag(111) values were taken from Ref. 7. The peak positions were determined visually and the peak width is a result of gaussian fittings corrected for instrumental broadening. The data range was $h\nu$ = 6-12 eV. Fitting the Ag(111) $h\nu$ = 8 eV spectrum with the functions used on the overlayer spectra produced values consistent with these.) Also, despite the obstruction of substrate peaks, the B^F values of the overlayer peak determined at nearby photon energies were consistent with those from $h\nu$ = 8 eV. The state has roughly the same binding energy as for Ag(111) but is much wider owing to the asymmetric tail on the higher binding energy side. This may be due to interaction between the adsorbate and substrate.

At 3 and 5 monolayer coverages, the angular dependence of the precursor surface state was investigated at $h\nu$ = 8 eV. All spectra were taken with the same parameters as shown in Figure 1, save that the ARPES analyzer was rotated off normal to obtain nonzero values of $k_{\parallel}$, the parallel component of crystal momentum. While no clean Cu(001) substrate off-normal spectra were available for direct comparison, the general appearance of the adsorbate spectra remained much the same, and the intensity of the precursor state was estimated by linearly extrapolating the diminishing background back up to the Fermi edge.

At 3 monolayers, rotating in the $\bar{\Gamma}$-$\bar{Y}$-$\bar{K}$ plane above and below the light polarization, the state was evident at $\theta_e = \pm 2^\circ$ ($k_{\parallel} = \pm$ 0.032 Å^{-1}) and at $\theta_e = \pm 5^\circ$ ($k_{\parallel} = \pm$ 0.079 Å^{-1}). In the $\bar{\Gamma}$-$\bar{\Sigma}$-$\bar{M}$ plane, the state was present at $\theta_e = \pm 2^\circ$, $\pm 5^\circ$, and $\pm 10^\circ$ ($k_{\parallel} = \pm$ 0.158 Å^{-1}), both toward

and away from the light polarization. Rotating the analyzer in the $\bar{\Gamma}$-$\bar{\Sigma}$-$\bar{M}$ plane toward the polarization of the synchrotron radiation ($\theta_e > 0$), at $\theta_e = 15^\circ$ ($k_\parallel = 0.236$ Å^{-1}) the precursor peak disappeared. At $\theta_e = 20^\circ$ ($k_\parallel = 0.312$ Å^{-1}), the peak reappeared. Within the precision of our measurements, the state does not appear to be dispersing as a function of $k_\parallel$. At a coverage of 5 monolayers, rotating in the $\bar{\Gamma}$-$\bar{\Sigma}$-$\bar{M}$ plane and toward the light polarization, the state was present at $\theta_e = 0^\circ$ and 2° but not at 5°. Again, there seems to be no dispersion with $k_\parallel$.

The behavior at 5 monolayers is consistent with that observed by Hansson and Flodstrom[13] in Ag(111) at $h\nu = 10.2$ eV ($k_\parallel < 0.103$ Å^{-1}). However, the three monolayer precursor seems to extend much further in $k_\parallel$ space. It appears that the precursor state may be restricted to a smaller area of the two-dimensional Surface Brillouin Zone as the overlayer becomes thicker and the valence bands become more three dimensional.

sp Plateau. The ratio of the sp plateau height to the valence band intensity is dependent upon the valence electronic structure of the system as discussed in Refs. 5 and 9. (In Ref. 7, it has been empirically shown that either the valence band maximum or integrated intensity can be used for this comparison.) The indirect transitions contributing to the sp plateau intensity are dependent upon the position of the bands near E_F, e.g., Band 6 of Ag(111). Figure 14 shows this ratio versus photon energy for clean Cu(001), 1-5 ML of c(10x) Ag/Cu(001), and Ag(111). As the exposure is increased, the behavior

of the ratio moves slowly toward that of Ag(111). This is yet another indication of the development of Ag(111)-like behavior in the metal overlayer. This specifically suggests that Band 6 is "slowly" developing in the silver overlayers, delayed by the hypothesized interaction of the sp states with the Cu(001) substrate.

Spectral Appearance. Finally, it is of interest to note the significant similarities between the spectra of Ag(111) and those of 5 ML c(10x2) Ag/Cu(001). As an example, those at 24 eV (Figure 4) bear a striking resemblance if the Cu features are neglected. Qualitatively, this is strong evidence for the approach of the valence structure of the c(10x2) Ag system toward that of bulk Ag(111).

V. CONCLUSIONS

Based upon the results of the LEED/AES calibration of Ref. 1 and the previous work discussed therein, the c(10x2) Ag/Cu(001) adlayer is assumed to be geometrically two-dimensional at coverages near 1 monolayer. It has been shown in the off-normal angle-resolved photoemission experiment of Ref. 1 that the monolayer structure is also electronically two-dimensional. Here, conclusive evidence is presented to document the development of the valence bands of the c(10x2) Ag from a two-dimensional to three-dimensional electronic structure. The three monolayer results demonstrate the importance of developing a crystal field similar to that of the bulk. Higher coverages are necessary to acquire sufficient periodicity in real space to observe dispersion in

the third dimension. By a coverage of 5 ML, the spectral behavior of the overlayer valence (and conduction) bands is very similar to that of Ag(111). This includes dispersion as a function of $k_\perp$, the Band 7 resonance, the constant kinetic energy feature, the Ag(111)-like surface state, the sp-plateau intensity profile, and, finally, the detailed visual appearance of the spectra themselves.

ACKNOWLEDGEMENTS

This work was supported by the Director, Office of Energy Research, Office of Basic Energy Sciences, Chemical Sciences Division of the U.S. Department of Energy under Contract No. DE-AC03-76SF00098. It was performed at the Stanford Synchrotron Radiation Laboratory, which is supported by the Department of Energy's Office of Basic Energy Sciences. J. G. Tobin acknowledges support by the National Science Foundation.

We also wish to acknowledge Mrs. Winifred Heppler for the preparation of the copper crystal and D. J. Trevor, C. C. Bahr, and J. J. Barton for their programs used in data reduction. Discussions with R. F. Davis and M. G. Mason were enlightening and greatly appreciated.

Appendix 1

A MODEL FOR Ag-ADSORBATE/Cu-SUBSTRATE PHOTOEMISSION RATIOS ASSUMING A LAYER-BY-LAYER GROWTH PATTERN[14]

SUBSTRATE

$$i_{Cu} = i^{o}_{Cu}\, e^{-z/z_o} \qquad (1)$$

i_{Cu}: photoemission intensity of the copper features including attenuation from the overlayer

i^{o}_{Cu}: photoemission intensity of the clean copper, bulk Cu(001)

z: overlayer thickness

z_o: escape depth of the substrate photoelectrons, through the adsorbate

NOTE: No correction for light attenuation

ADSORBATE

$$j_{Ag} = \sum_{k=1}^{n} j^{k}_{Ag} \qquad (2)$$

j_{Ag}: photoemission intensity from the silver overlayer

j^{k}_{Ag}: photoemission intensity from the kth monolayer of an overlayer slab n monolayers thick

$$j^{k}_{Ag} = j^{1}_{Ag}\, e^{-(k-1)t/t_o} \qquad (3)$$

j^{1}_{Ag}: photoemission intensity from the topmost monolayer of the overlayer, k = 1

t: thickness of one monolayer

(k-1)t: thickness of the overlayer above the kth monolayer

t_o: escape depth of the adsorbate electrons, through the adsorbate

NOTE: $z = nt$ (4)

$$R_n = \frac{j_{Ag}}{i_{Cu}} = \frac{j^1_{Ag}}{i^o_{Cu}} \sum_{k=1}^{n} \frac{e^{-(k-1)t/t_o}}{e^{-z/z_o}} \tag{5}$$

In the case of an overlayer only one monolayer thick: k=n=1, z=t

$$R_1 = \frac{j^1_{Ag}}{i^o_{Cu}} \frac{1}{e^{-t/z_o}} \tag{6}$$

Defining a ratio normalized to the ratio at 1 ML:

$$R'_n = \frac{R_n}{R_1} = \sum_{k=1}^{n} \frac{(e^{-(k-1)t/t_o})\,(e^{z/z_o})}{e^{t/z_o}} \tag{7}$$

Substituting z=nt and setting $t_o = z_o$ (same kinetic energy range)

$$R'_n = \sum_{k=1}^{n} \frac{e^{-(k-1)t/z_o}}{e^{-(n-1)t/z_o}} \tag{8}$$

Eq. (8) Eq. (8) was used to calculate the theoretical values of Table II.

REFERENCES

1. J.G. Tobin, S.W. Robey, and D.A. Shirley, Phys. Rev. B 33, 2270 (1986) and references therein. This article contains a rather extensive listing of pertinent studies.

2. P. Heimann, H. Neddermeyer, and H.F. Roloff, Proceedings of the 7th International Vacuum Congress and the Third International Conference on Solid Surfaces, Vienna, Austria, 1977.

3. F.J. Arlinghaus, J.G. Gay, and J.R. Smith, Phys. Rev. B 20, 1332 (1979); Phys. Rev. B 25, 643 (1982).

4. J.G. Tobin, S.W. Robey, L.E. Klebanoff, and D.A. Shirley, Phys. Rev. B 28, 6169 (1983).

5. J.G. Nelson, S. Kim, W.J. Gignac, R.S. Williams, J.G. Tobin, S.W. Robey, and D.A. Shirley, Phys. Rev. B 32, 3465 (1985).

6. S.D. Kevan and D.A. Shirley, Phys. Rev. B 22, 542 (1980).

7. J.G. Tobin, Ph.D. Thesis, University of California, Berkeley, 1983.

8. D.P. Spears, R. Melander, L.G. Petersson, and S.B.M. Hagstrom, Phys. Rev. B 21, 1462 (1980).

9. P.S. Wehner, R.S. Williams, S.D. Kevan, D. Denley, and D.A. Shirley, Phys. Rev. B 19, 6164 (1979).

10. S.-T. Lee, G. Apai, M.G. Mason, R. Benbow, and Z. Hurych, Phys. Rev. B 23, 505 (1981).

11. G. Apai, S.-T. Lee, and M.G. Mason, Solid State Communications 37, 212 (1981).

12. M.O. Krause, P.R. Woodruff, and T.A. Carlson, J. Phys. B 14, L673 (1981); M.O. Krause, J. Chem. Phys. 72, 6474 (1980).

13. G.V. Hansson and S.A. Flodstrom, Phys. Rev. B 17, 473 (1978).

14. G. Ertl and J. Kuppers, "Low Energy Electrons and Surface Chemistry," Verlag-Chemie, 1974, pages 39-40.

15. P.S. Wehner, Ph.D. Thesis, University of California, Berkeley, 1978; C.R. Brundle, J. Vac. Sci. Technol. 11, 212 (1974).

TABLE CAPTIONS

Table 1. The spectrometer work functions for the adlayer systems and Ag(111).

Table II. This is a summary of the observed and predicted Ag/Cu photoemission intensity ratios and the ratio of the experimental to theoretical values. They are normalized to the 1 ML value, such that $R'_n = R_n/R_1$ with $R_n = (j_{Ag}/i_{Cu})_n$. The subscript n represents the exposure in ML. The thickness of a monolayer is defined as t and assumed to be approximately 2.5 Å. The escape depth of an electron of a given kinetic energy is z_o. These were taken from the "Universal Curve" of electron escape depths.[15] Appendix 1 has a derivation of the attenuation model.

Table III. Comparison of the binding energies with respect to the Fermi energy and the full widths at half maximum (FWHM) of the Ag(111) surface state and its precursor observed in c(10x2) Ag/Cu(001). All overlayer measurements were derived from data collected at normal emission for $h\nu$ = 8 eV. The Ag(111) data is from Refs. 5 and 7.

Table I. Spectrometer work functions

Exposure (ML)	AVE φ_{AN} (eV)	± Standard Deviation (eV)
0	4.53	± 0.03
1	4.52	± 0.02
2	4.49	± 0.08
3	4.57	± 0.06
4	4.53	± 0.02
5	4.52	± 0.02
AVE ± S.D.	4.53	± 0.03
Ag(111)	4.55	± 0.02

Table II. Ag/Cu Photoemission Ratios

$h\nu$ (eV)	z_o (Å)	t/z_o		R'_1	R'_2	R'_3	R'_4	R'_5	AVE ± S.D.
			Exp. 1		2.9	3.9	4.6	6.3	
16	15	1/6	Theory 1		2.2	3.6	5.2	7.2	
			Ratio=EXP/TH	1.3	1.1	0.9	0.9		1.0 ± 0.2
			Exp. 1		2.9	4.7	5.5	8.7	
21	10	1/4	Theory 1		2.3	3.9	6.0	8.8	
			Ratio=EXP/TH	1.3	1.2	0.9	1.0		1.1 ± 0.2
			Exp. 1		3.6	6.2	5.2	7.4	
32	7.5	1/3	Theory 1		2.4	4.3	7.1	10.9	
			Ratio=EXP/TH	1.5	1.4	0.7	0.7		1.1 ± 0.4
	5	1/2	Theory 1		2.6	5.4	9.8	17.2	
			Ratio=EXP/TH	1.4	1.1	0.5	0.4		0.85 ± 0.5

Table III. Surface State

	B^F (eV)	Width (eV)
Ag(111)	0.065 ± 0.004	0.111 ± 0.007
Monolayers of c(10x2) Ag/Cu(001)		
5	0.10	0.7
4	0.11	1.0
3	0.14	1.2
2	0.11	1.4

FIGURE CAPTIONS

Figure 1. The geometry of the photoemission experiment is illustrated here: top - the real space relationships; bottom - the Surface Brillouin Zones in reciprocal space and their relationships to the plane containing the polarization $\vec{A}$. The surface normal, $\vec{n}$, the light polarization and the Poynting vector of the light are all in the horizontal plane.

Figure 2. The ARP spectra taken at $h\nu$ = 6, 7, and 8 eV are plotted versus the binding energy (B^F) with respect to the Fermi level (E_F). The spectra are normalized to the largest feature in each spectrum. Cu(001) is at the bottom, followed sequentially upward by the spectra of c(10x2) Ag/Cu(001) of 1/2, 1, 2, 3, 4, and 5 monolayer exposures. The bulk, single-crystal Ag(111) spectrum is topmost. All of the data was collected at normal emission, either parallel to [001] of Cu(001) or [111] of Ag(111). In the 8 eV plot, the Ag(111) spectrum was expanded to more fully illustrate the surface state near E_F.

Figure 3. Same as Figure 2 with $h\nu$ = 14 eV.

Figure 4. Same as Figure 2 with $h\nu$ = 24 eV.

Figure 5. Same as Figure 2 with $h\nu$ = 28 eV.

Figure 6. Same as Figure 2 with $h\nu$ = 30 eV.

Figure 7. This is a plot of the binding energy (B^F) with respect to the Fermi Level (E_F) of the silver overlayer features at one monolayer exposure versus the photon energy.

Figure 8. Same as Figure 7 but for an exposure of two monolayers.

Figure 9. Same as Figure 7 but for an exposure of three monolayers.

Figure 10. Same as Figure 7 but for an exposure of four monolayers.

Figure 11. Same as Figure 7 but for an exposure of five monolayers.

Figure 12. Same as Figure 7 but for Ag(111).

Figure 13. The ratio of the intensity of the high B^F half of the silver valence bands to the intensity of the low B^F half of the silver bands, plotted as a function of photon energy for the samples Ag(111) (filled circles) and five (filled triangles) and four monolayers (filled squares) of c(10x2) Ag/Cu(001). The ratio of the 5 ML values (including the RMS deviation) to the Ag(111) values is 0.57 ± 0.09. The ratio of the 4 ML values to the Ag(111) values is 0.52 ± 0.09 and to the 5 ML values is 0.92 ± 0.07.

Figure 14. The ratio of the sp plateau height to the valence band maximum, versus photon energy, for Cu(001), 1, 2, 3, 4, and 5 ML of c(10x2) Ag/Cu(001), and Ag(111).

ARP Diagram

$\theta_e = 0°$

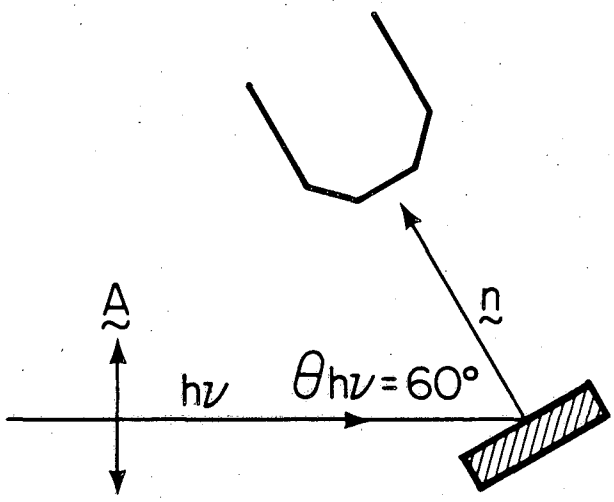

Surface Brillouin Zones

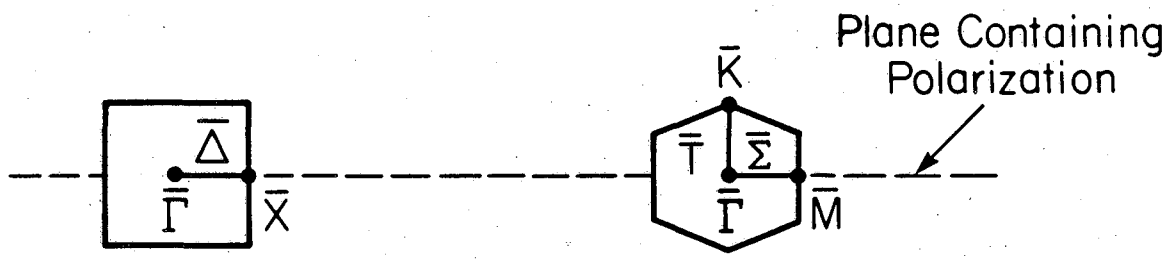

Cu (001)
$\bar{X} = 1.23 Å^{-1}$

c(10x2)Ag And Ag(111)
$\bar{M} = 1.25 Å^{-1}$

XBL837-981

Figure 1

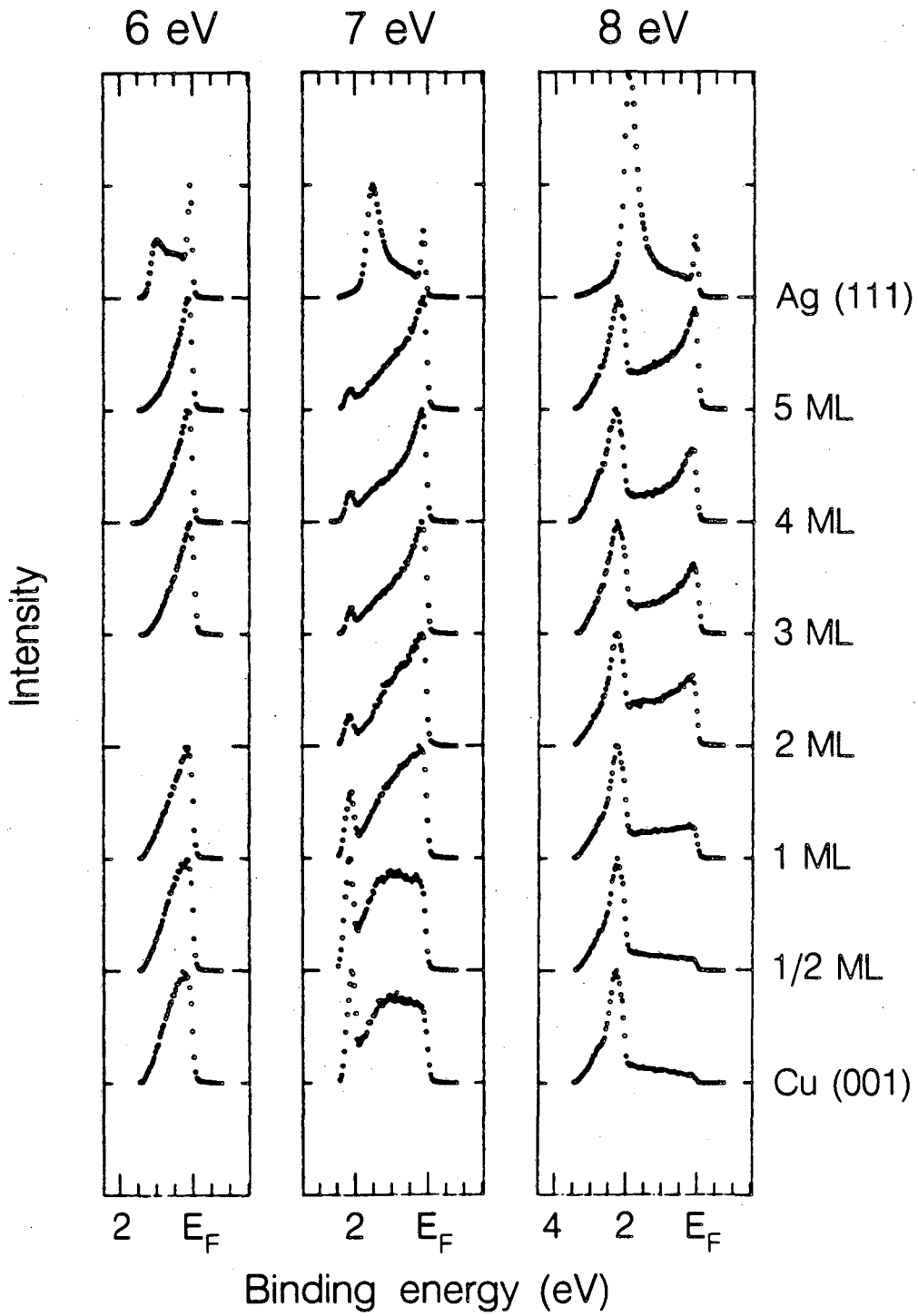

XBL 835-9923A

Figure 2

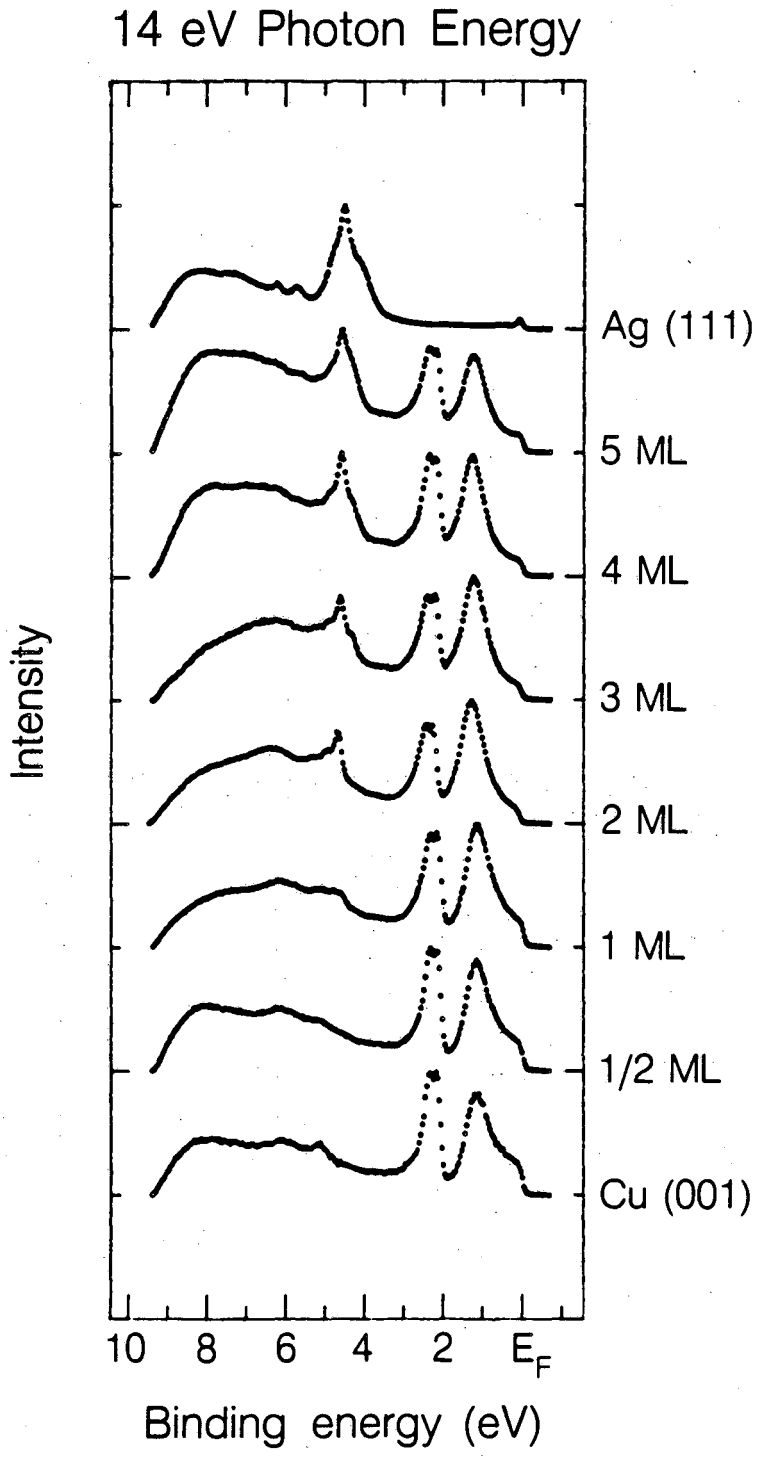
14 eV Photon Energy
Intensity
Ag (111)
5 ML
4 ML
3 ML
2 ML
1 ML
1/2 ML
Cu (001)
10
8
6
4
2
E_F
Binding energy (eV)
XBL 835-9926A

Figure 3

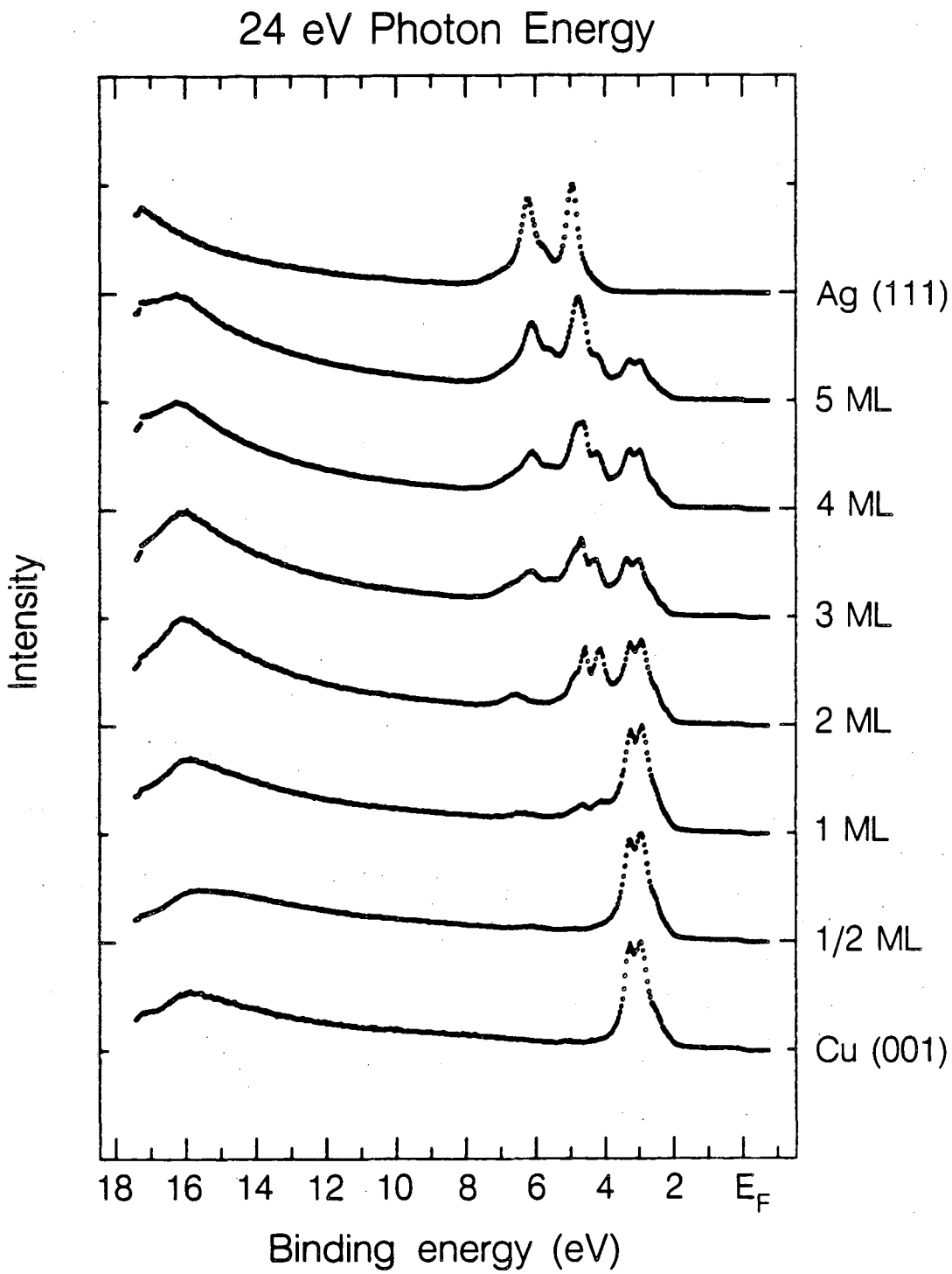

XBL 835-9933A

Figure 4

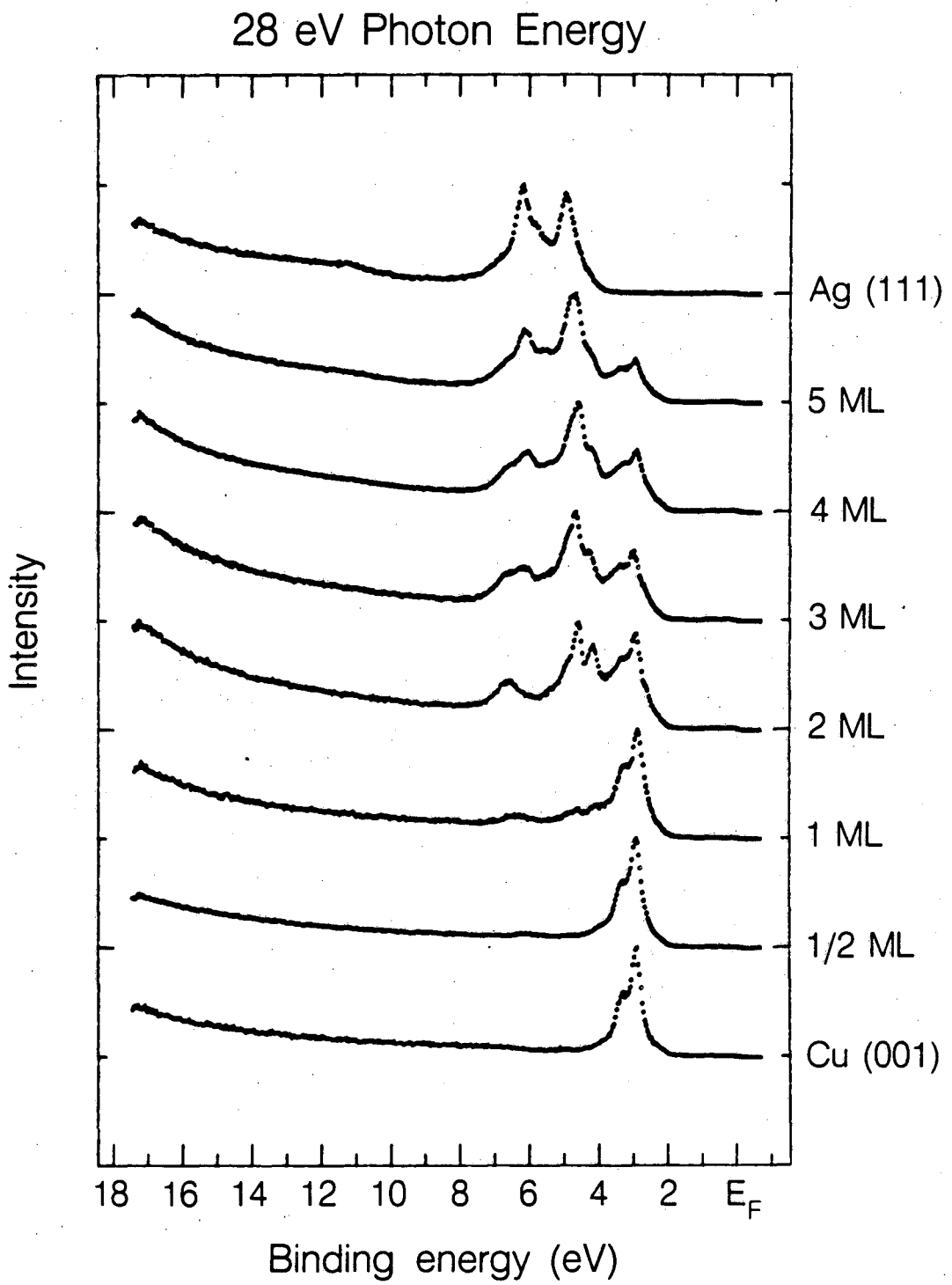
28 eV Photon Energy
Intensity
Ag (111)
5 ML
4 ML
3 ML
2 ML
1 ML
1/2 ML
Cu (001)
18 16 14 12 10 8 6 4 2 E_F
Binding energy (eV)
XBL 835-9935A

Figure 5

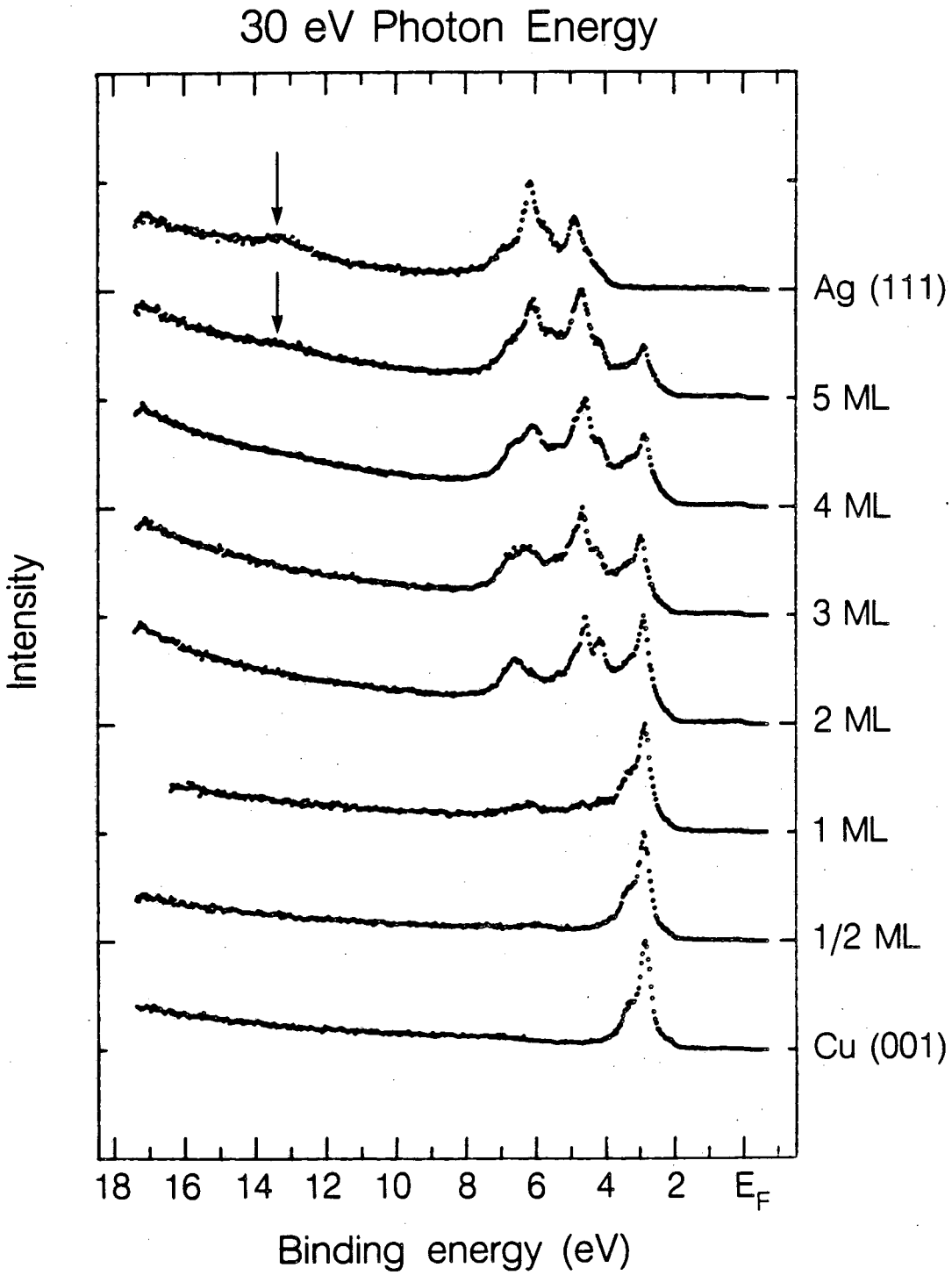

XBL 835-9936 Z

Figure 6

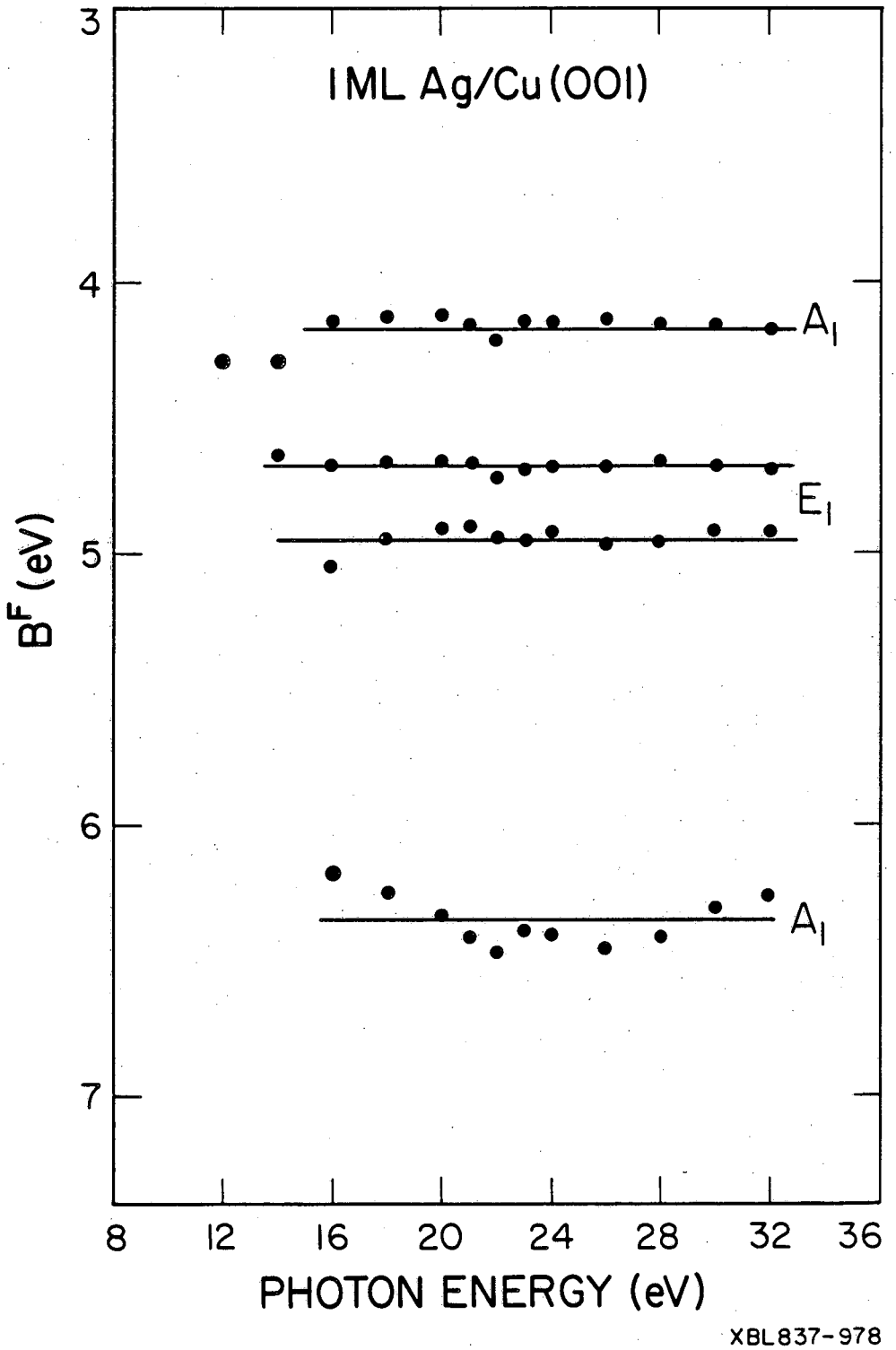
1ML Ag/Cu(001)
3
4
5
6
7
B^F (eV)
A_1
E_1
A_1
8
12
16
20
24
28
32
36
PHOTON ENERGY (eV)
XBL837-978

Figure 7

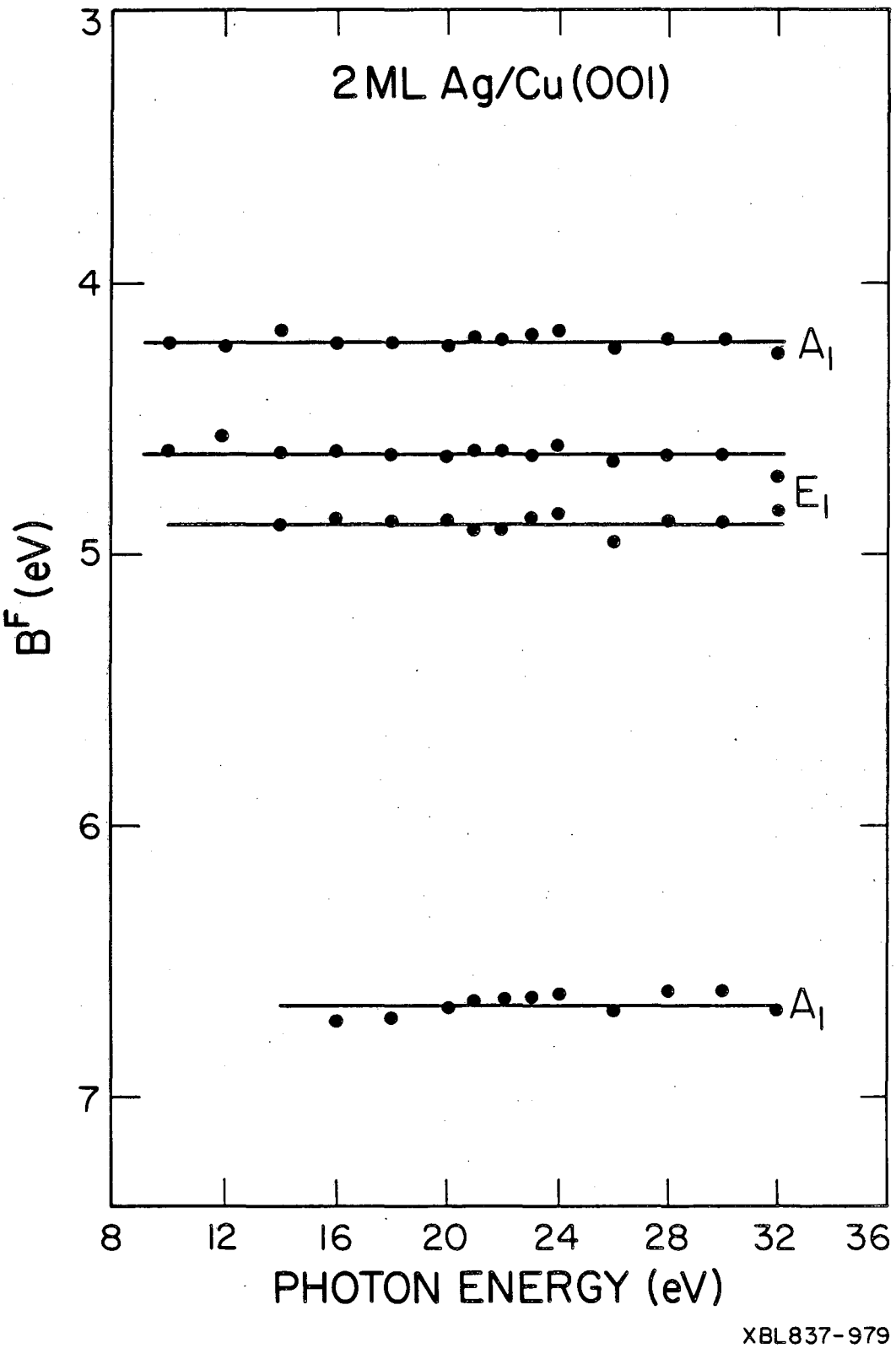
2 ML Ag/Cu(001)
B^F (eV)
3
4
5
6
7
A_1
E_1
A_1
8
12
16
20
24
28
32
36
PHOTON ENERGY (eV)
XBL837-979

Figure 8

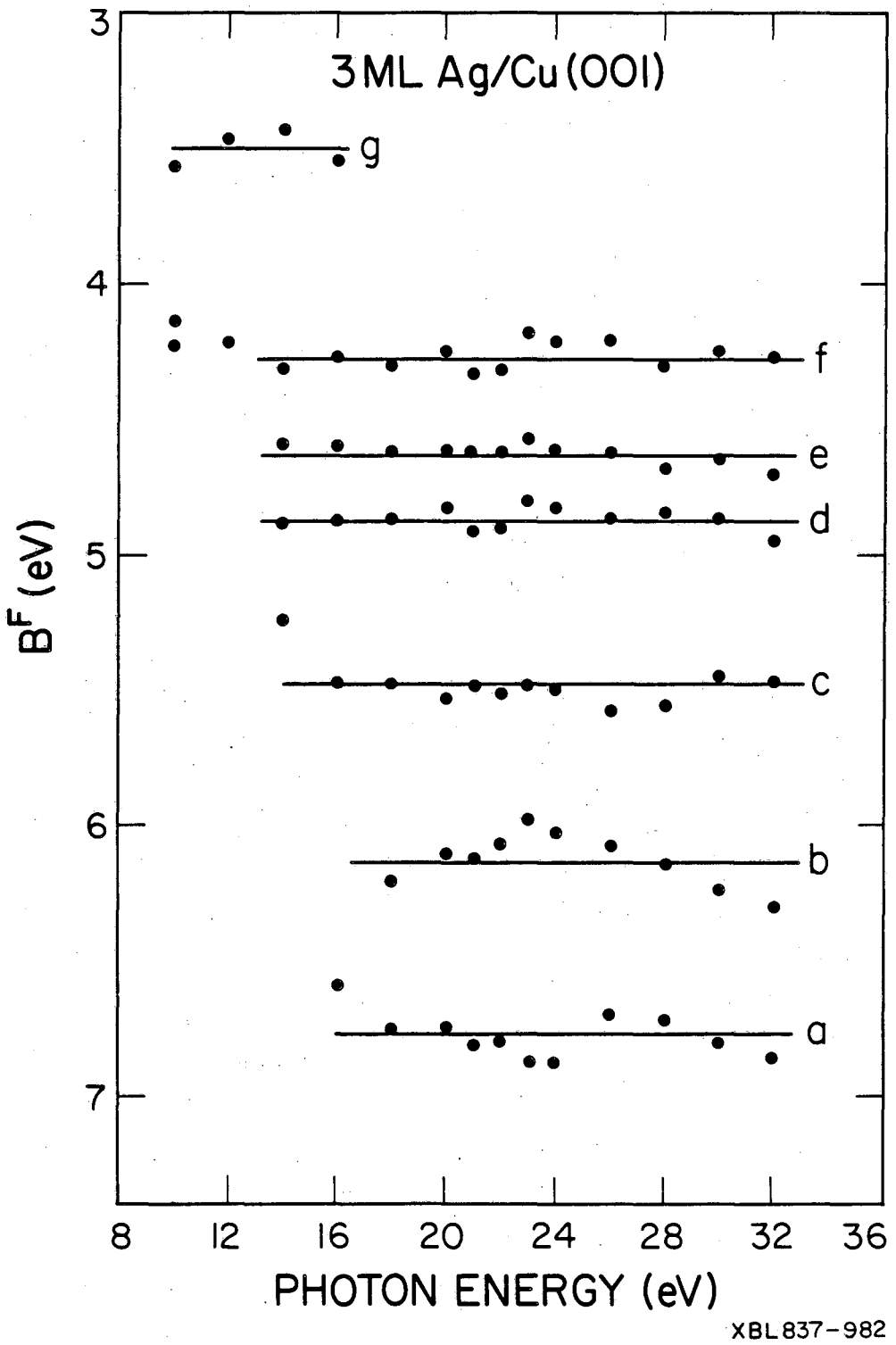
3ML Ag/Cu(001)
g
f
e
d
c
b
a
B^F (eV)
3
4
5
6
7
8
12
16
20
24
28
32
36
PHOTON ENERGY (eV)
XBL837-982

Figure 9

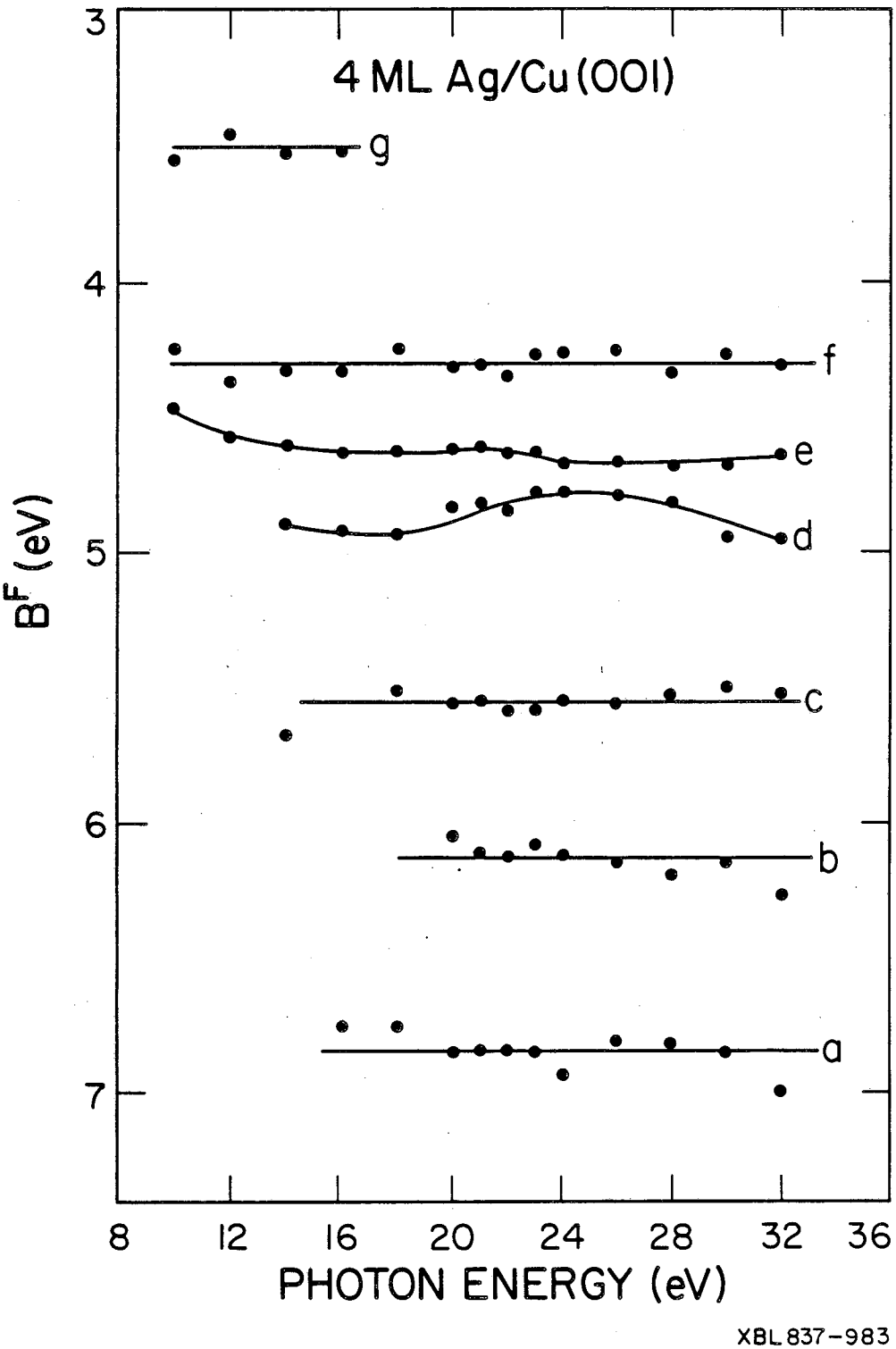
4 ML Ag/Cu(001)
g
f
e
d
c
b
a
B^F (eV)
3
4
5
6
7
8
12
16
20
24
28
32
36
PHOTON ENERGY (eV)
XBL 837-983

Figure 10

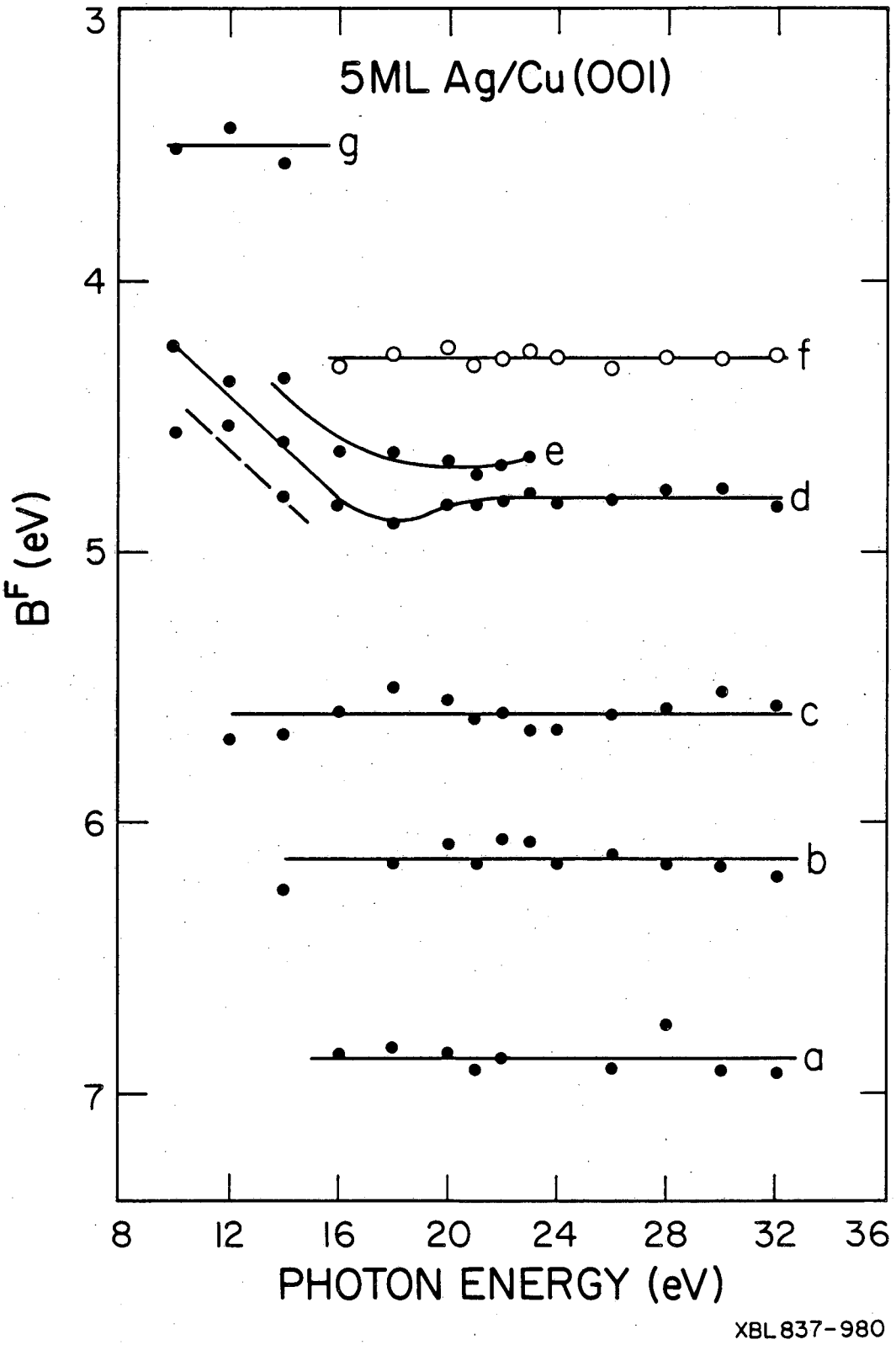
5ML Ag/Cu(001)
g
f
e
d
c
b
a
B^F (eV)
3
4
5
6
7
8
12
16
20
24
28
32
36
PHOTON ENERGY (eV)
XBL837-980

Figure 11

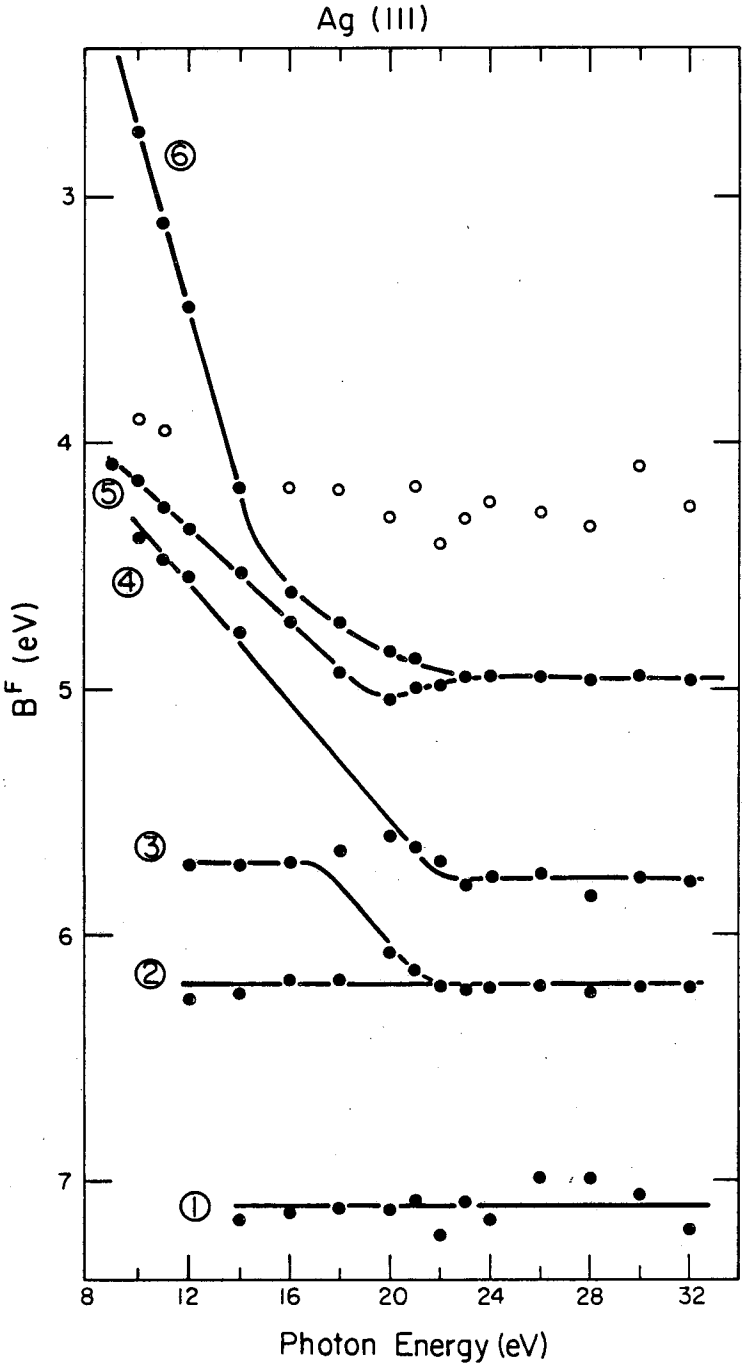
Ag (111)
⑥
⑤
④
③
②
①
3
4
5
6
7
B^F (eV)
8
12
16
20
24
28
32
Photon Energy (eV)
XBL 837-976

Figure 12

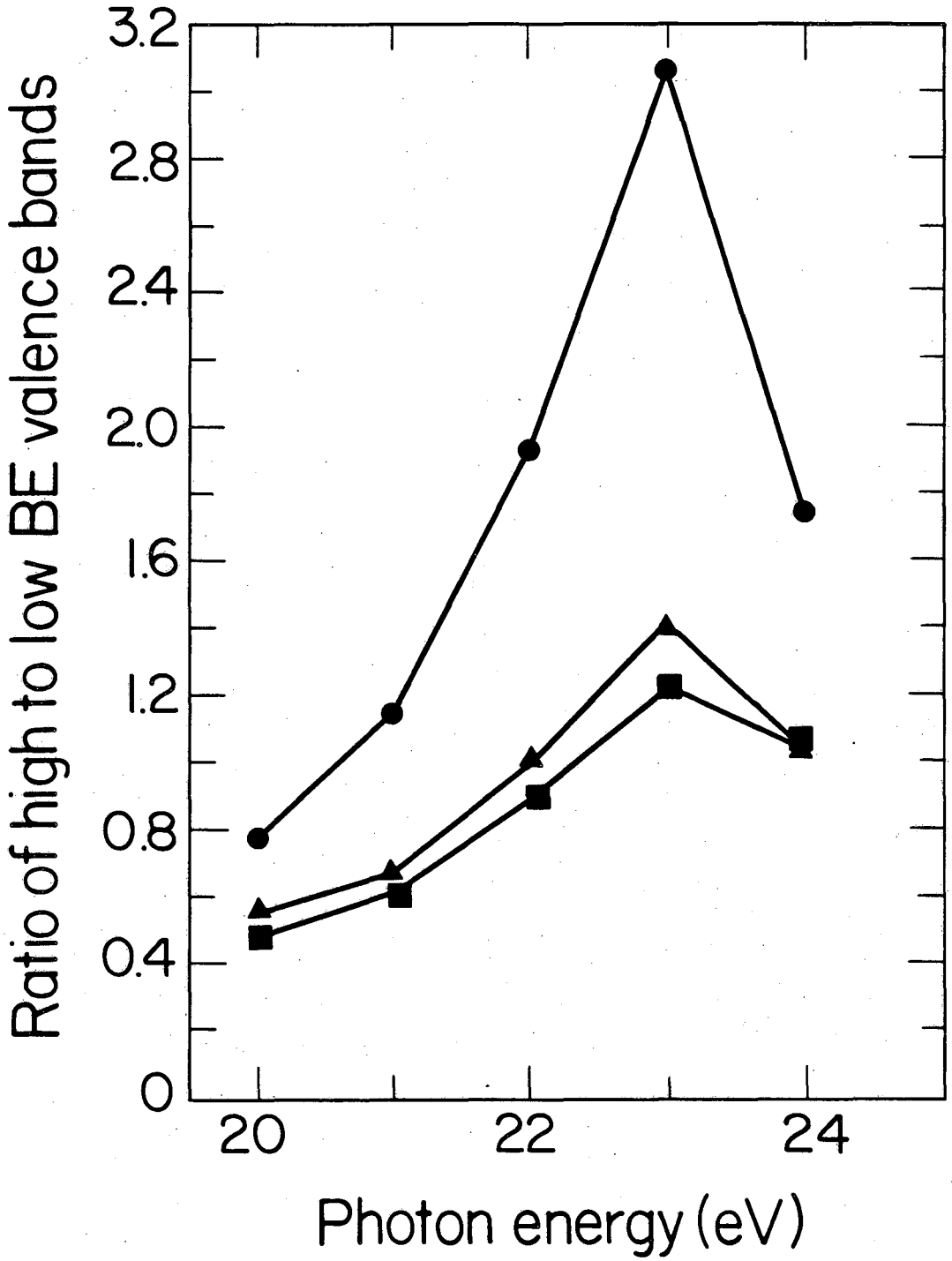
Ratio of high to low BE valence bands
3.2
2.8
2.4
2.0
1.6
1.2
0.8
0.4
0
20
22
24
Photon energy (eV)
XBL 833-106

Figure 13

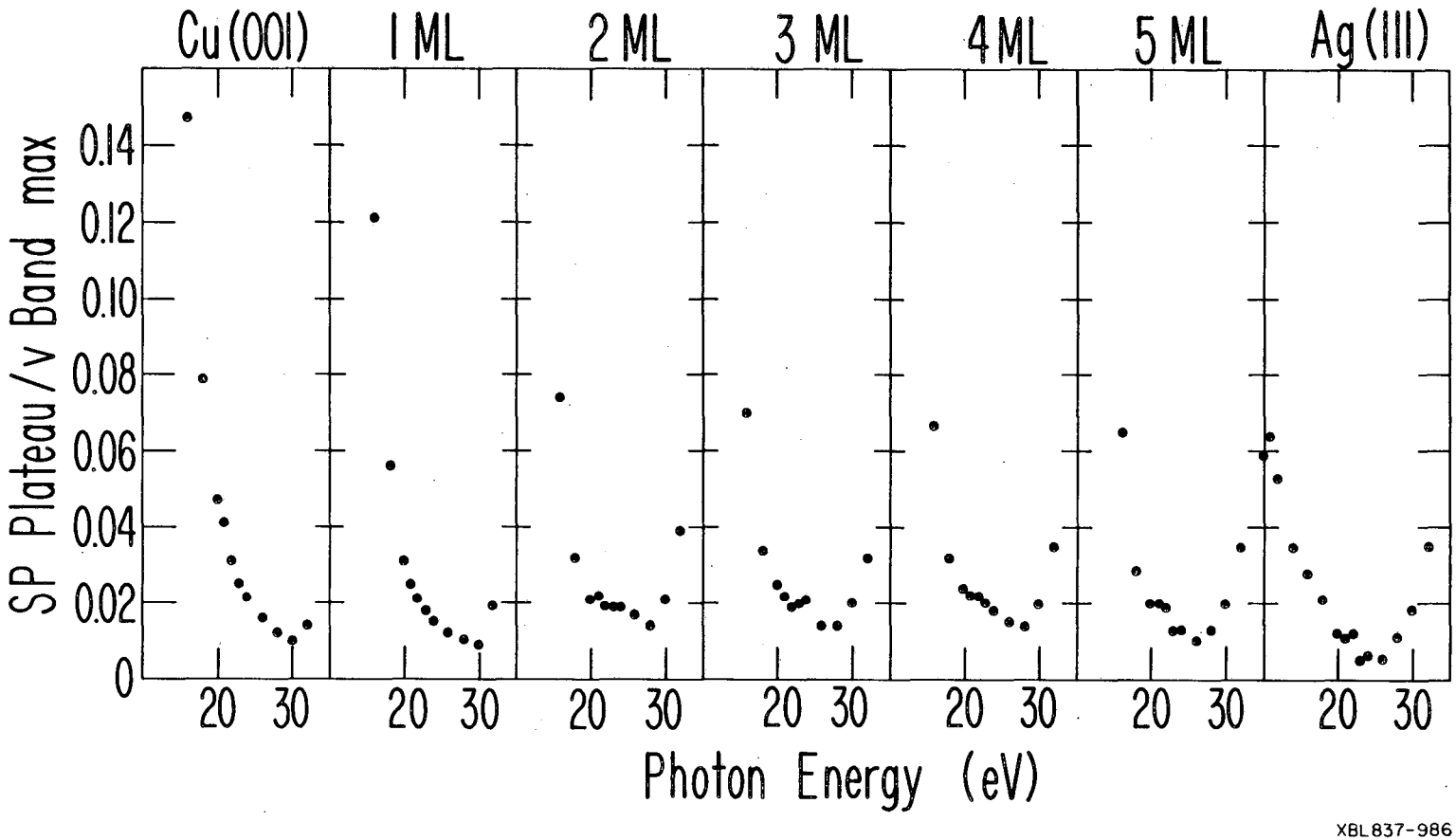
Cu(001)
1 ML
2 ML
3 ML
4 ML
5 ML
Ag(111)
SP Plateau / v Band max
0.14
0.12
0.10
0.08
0.06
0.04
0.02
0
20
30
Photon Energy (eV)
XBL837-986

Figure 14

LAWRENCE BERKELEY LABORATORY
TECHNICAL INFORMATION DEPARTMENT
UNIVERSITY OF CALIFORNIA
BERKELEY, CALIFORNIA 94720